The Influence of Transverse Tubular Delays on the Kinetics of Charge Movement in Mammalian Skeletal Muscle

BRUCE J. SIMON and KURT G. BEAM

From the Department of Physiology and Biophysics, University of Iowa School of Medicine, Iowa City, Iowa 52242

ABSTRACT A model was developed to describe the kinetics of slow, voltage-dependent charge movement in the rat omohyoid muscle. To represent the electrically distributed nature of the transverse tubular system (t-system), we followed an approach similar to that described by Adrian and Peachey (1973 *J. Physiol.* [*Lond.*]. 235:103), and approximated the fiber with 12 concentric cylindrical shells. Incorporated into each shell were capacitative and conductive elements that represented the passive electrical properties of the t-system, and an element representing the mobile charge. The charge was assumed to obey a two-state scheme, in which the redistribution of charge is governed by a first-order reaction, and the rate constants linking the two states were assumed to depend on potential according to the constant field expression. The predictions of this "distributed two-state model" were compared with charge movements experimentally measured in individual fibers. For this comparison, first, the passive electrical parameters of the model were adjusted to fit the experimental linear capacity transient. Next, the Boltzmann expression was fitted to the steady state Q vs. V data of the fiber, thereby constraining the voltage dependence of the rate constants, but not their absolute magnitude. The absolute magnitude was determined by fitting the theory to an experimental charge movement at a single test potential, which in turn constrained the fits at all other test potentials. The distributed two-state model well described the rising and falling phases of ON, OFF, and stepped OFF charge movements at temperatures ranging from 3 to 25°C. We thus conclude that tubular delays are sufficient to account for the rounded rising phase of experimental charge movements, and that it is unnecessary to postulate higher-order reaction schemes for the underlying charge redistribution.

INTRODUCTION

A large, slow asymmetry current measured after the blockade of ionic currents in vertebrate skeletal muscle has been implicated in excitation-contraction (E-C)

Address reprint requests to Dr. Kurt G. Beam, Dept. of Physiology and Biophysics, University of Iowa School of Medicine, Iowa City, IA 52242. Dr. Simon's present address is Dept. of Physiology, University of Rochester Medical Center, Rochester, NY 14642.

J. GEN. PHYSIOL. © The Rockefeller University Press · 0022-1295/85/01/0021/22$1.00

Volume 85 January 1985 21–42

coupling. This current, usually called "charge movement," has been hypothesized (Schneider and Chandler, 1973) to represent the molecular rearrangement of a charged structure that lies at least partially within the transverse tubular membrane and has the function of coupling the depolarization of the t-system to the release of calcium from the sarcoplasmic reticulum (SR). The previous paper (Simon and Beam, 1985) described charge movements measured in the rat omohyoid muscle. These charge movements were found to be similar to charge movements in frog twitch muscle (Chandler et al., 1976; Adrian and Almers, 1976) and in rat extensor digitorum longus (EDL) muscle (Hollingworth and Marshall, 1981; Dulhunty and Gage, 1983). In order to understand the role charge movement may play in the gating of calcium release from the SR, it is necessary to understand the reaction scheme that governs the movement of the charge. This paper presents a model that quantitatively accounts for the kinetics of charge movement.

The simplest reaction scheme is one in which the charge moves back and forth between two states. For a step in potential, a two-state scheme predicts a current that rises instantaneously and then decays exponentially. By contrast, experimentally measured charge movements typically have a slow rising phase and a rounded peak, and it is not until several milliseconds after the step in potential that the charge transient begins to decay exponentially. A possible explanation for this slow rising phase is that it is due to the movement of the charge in several sequential steps. A specific multistate reaction scheme for charge movement has been proposed by Horowicz and Schneider (1981) and was shown by them to give a good account of the kinetics of ON transients in frog muscle. We have confirmed that the model of Horowicz and Schneider also accounts for the kinetics of ON transients in the rat omohyoid muscle; however, we have shown (Simon and Beam, 1983*a*) that it fails to account for transients evoked by a stepped OFF pulse protocol, a protocol not tested by Horowicz and Schneider. This failure prompted us to search for alternative descriptions for the kinetics of charge movement.

Determining whether a two-state or multistate reaction scheme best describes charge movement is complicated by the presumed tubular location of the mobile charge. The voltage clamp controls the potential at the surface of the fiber, and in order to change potential within the t-system, it must charge the tubular membrane through the series resistance presented by the tubular lumen. The total series resistance is largest for those portions of the t-system farthest from the surface. Thus, the change in potential within the t-system will lag the change on the surface, and this lag will be greater for portions of the t-system farther from the surface. Not only will the propagation of voltage into the fiber be delayed, but also the current produced by the movement of charge within the t-system will be delayed in its appearance at the surface of the fiber where it is measured. Experimental support for the importance of such tubular propagation delays to the kinetics of charge movement is provided by the effects of temperature described in the previous paper (Simon and Beam, 1985).

To quantify the effects of t-tubular delays on the kinetics of charge movement, it is necessary to have a representation of the electrically distributed nature of

the t-system. Toward this end, we have constructed a model of the muscle fiber similar to that described by Adrian and Peachey (1983), but modified to incorporate the effects of the mobile charge in the t-tubular membranes. The mobile charge was assumed to obey a two-state model. Because a two-state model predicts that a step in potential will cause a current that rises instantaneously with no delay, the use of such a model permits one to determine whether tubular delays alone are sufficient to account for the delays in measured charge movements, or whether a more complicated, multistate model for charge movement is required. We determined that a multistate scheme is unnecessary since a two-state model distributed throughout the t-system gives a good account of both the rising and falling phases of measured charge movements.

An abstract describing some of these results has appeared (Simon and Beam, 1983*b*).

METHODS

The Distributed Two-State Model

In our model, we have followed the general approach used by Adrian and Peachey (1973) to reconstruct action potentials in frog muscle. The fiber is represented, in cross section, as a series of concentric annuli. Each annulus is represented by a parallel combination of a conductance and a capacitance, which correspond to the passive properties of the t-tubular wall. A third element, in parallel with the conductance and capacitance, accounts for the nonlinear charge movement across the tubular wall. Neighboring annuli are linked together by a conductance that represents the current pathway within the lumen of the t-system, with the outermost annulus being separated from the surface of the fiber by an access resistance. For simplicity in our calculations, we have assumed that the leak conductance of the t-tubular wall is negligible (see Discussion), and that no time-dependent ionic currents flow across the surface or t-tubular membranes.

Our approach differs from that of Adrian and Peachey (1973) in that they used annuli that divided the fiber cross section into equal radial increments, whereas we have used annuli that divide the cross section into equal areas. Specifically, for N annuli and a fiber of radius a, the nth annulus has inner and outer radii of $a\sqrt{(n-1)/N}$ and $a\sqrt{n/N}$, respectively ($n = 1$ to N). The voltage of the nth annulus, V_n, was taken at the point, r_n, with equal areas on either side. That is,

$$r_n = a\sqrt{(n - \tfrac{1}{2})/N},$$

with the conventions that

$$r_1 = 0 \quad \text{and} \quad r_{N+1} = a.$$

The conductance, g_n, linking the nth and $n + 1$st annuli is:

$$g_n = \frac{\pi(r_{n+1} + r_n)\bar{G}_l}{(r_{n+1} - r_n)}, \tag{1}$$

where $\bar{G}_l$ is the conductance of the lumen of the t-system per unit fiber volume. The capacitance of each annulus is

$$C_n = \bar{C}_w(\pi a^2/N),$$

where $\bar{C}_w$ is the capacitance of the t-system per unit fiber volume.

The change in voltage across the capacitance of the nth annulus, caused by current flowing between it and the two adjacent annuli, was calculated according to the difference equation:

$$C_n(dV_n/dt) = (V_{n+1} - V_n)g_n - (V_n - V_{n-1})g_{n-1} - dQ_n/dt, \quad (2)$$

where the calculation of dQ_n/dt, the nonlinear charge movement associated with the nth annulus, is described below. N such difference equations were solved simultaneously to give V_n for each annulus as a function of time. That is, the values of V_n at time t were used to compute dV_n/dt at each annulus by means of Eq. 2. V_n at time $t + h$, where h is a small increment in time, was then calculated according to:

$$V_n(t + h) = V_n(t) + hdV_n(t)/dt, \quad (3)$$

and the process was repeated. The current flowing into a unit length of fiber, I, was then calculated according to:

$$I = (V_s - V_N)/(2\pi aR_a + 1/g_N), \quad (4)$$

where V_s is the voltage at the surface of the fiber, g_N is the lumen conductance calculated with Eq. 1, and R_a is the "access" resistance between the surface and the outermost annulus. $V_s(t)$ was expressed as:

$$V_s(t) = V_f + (V_i - V_f)\exp(-t/\tau_c),$$

where V_i and V_f are the initial and final potentials, and τ_c is the time constant for the change in potential produced by the voltage clamp. Experimentally, the controlled potential (at the V_1 electrode) was found to rise exponentially with a time constant varying between 0.3 and 0.4 ms (see Fig. 1*B* in Simon and Beam, 1983*a*). An average τ_c of 0.35 ms was used in all of the modeling.

The Kinetic Model for the Underlying Charge Redistribution

The density of mobile charge was assumed to be uniform throughout the t-system, proportional to the t-tubular area of each annulus. The charge was assumed to obey a two-state reaction scheme and to respond to a potential change across the t-tubule membrane by redistributing between the two states according to the first-order differential equation:

$$dB/dt + (\alpha + \beta)B = \alpha, \quad (5)$$

where α and β, the forward and reverse rate constants, are instantaneous functions of voltage, and B is the fraction of total charge in the state that becomes populated during depolarization. In the steady state, B is given by the Boltzmann expression:

$$B = 1/[1 + \exp(-\phi)]; \qquad \phi = (V - \bar{V})/k, \quad (6a, b)$$

where $\bar{V}$ is the potential at which both states are equally occupied and k is a steepness factor that depends on the valence of the charge. The amount of charge that moves, Q, is equal to BQ_{max}.

The solution to Eq. 5 for a step in potential is:

$$B = B_f + (B_i - B_f)\exp[-t(\alpha + \beta)], \quad (7)$$

where B_i and B_f are the initial and final values of B.

The rate constants, α and β, were assumed to depend on potential according to a constant field diffusion model (Chandler et al., 1976; Benz and Zimmermann, 1983):

$$\alpha = \bar{\alpha}\phi/[1 - \exp(-\phi)]; \qquad \beta = \alpha \exp(-\phi), \tag{8}$$

from which $\tau = 1/(\alpha + \beta)$ is calculated as:

$$\tau = (2\bar{\tau}/\phi)\tanh(\phi/2), \tag{9}$$

where ϕ is given by Eq. 6*b* and $\bar{\alpha}$ and $\bar{\tau}$ are the values of α and τ at $\phi = 0$.

For a step to a given potential, the asymmetry current related to voltage-dependent charge movement was obtained as the difference between the "test" current transient generated by Eq. 2, and the linear "control" current transient generated by Eq. 2 with $dQ_n/dt = 0$. This is analogous to the procedure used experimentally (Simon and Beam, 1985), except that the experimental control current was measured for a voltage step from −135 to −90 mV and then appropriately scaled and subtracted from the test current.

Fitting Computer-generated Charge Movements to Experimental Data

The distributed two-state model summarized by Eqs. 1–9 was implemented in a computer program that was written in Fortran IV and run in double precision (16 decimal places) on a VAX 11/780 minicomputer (Digital Equipment Corp., Maynard, MA). The computed charge movements were compared with experimental charge movements, which were measured in the rat omohyoid muscle as described in the preceding paper. The small delay (~100 μs) added to the experimental records by electronic filtration (four-pole, low-pass Bessel, f_{cutoff} = 4 kHz) was ignored in the modeling. All the theoretical curves illustrated in this paper were calculated using 12 annuli and an integration time increment (cf. Eq. 3) of 0.5 μs.

The first step in applying the theory was to fit the calculated linear capacity transient to the measured transient. In the model, the passive electrical properties of the t-system are governed by four parameters, the fiber radius a, R_a, $\bar{G}_l$, and $\bar{C}_w$ (cf. Eqs. 1, 2, and 4). In principle, one could measure the radius of each fiber as well as the morphometric parameters of the t-system that are necessary in order to calculate $\bar{G}_l$ and $\bar{C}_w$. In fact, an accurate visual determination of fiber radius is difficult and the morphometric measurements of t-system for each fiber are impractical. Hence, we chose to fix the fiber radius at 32 μm, the average diameter of the predominant fiber type in the omohyoid muscle (Müntener et al., 1980), and to fix the parameters C_w, ρ, and ζ, which define $\bar{C}_w$, at values (Table I) that yield a total fiber capacitance in agreement with the previously measured values reported in the literature (see Discussion). Various combinations of the remaining two parameters, R_a and $\bar{G}_l$, were found to give excellent fits to the linear capacity transient, but an access resistance of 60 Ω·cm² resulted both in the best fits to the charge movement data (see Results) and in values for G_l similar to the value used by Adrian and Peachey (1973). Therefore, the access resistance was fixed at 60 Ω·cm² and in order to fit the experimental capacity transient of a given fiber, only $\bar{G}_l$ was varied. The capacitance of the fiber's surface was fixed at 1 μF/cm². This choice affects the first 250–500 μs of the calculated linear capacity transient but little affects the value of $\bar{G}_l$ that gives the best overall fit to the experimental linear capacity transient, and thus does not affect the time course of the calculated charge movements.

The choice of a fixed radius and fixed morphometric parameters for the t-system means that computations were carried out in terms of an idealized fiber with a total linear capacitance of 5.8 μF/cm² (Table I). Because the fiber radius and t-system geometry vary from fiber to fiber, the actual linear capacitance also varies. Thus, in order to compare the kinetics of the calculated and measured linear capacity transients, the amplitude of the theoretical curve was scaled to match that of the measured transient. We preferred to use a standard set of geometric parameters rather than to adjust these parameters to

fit individual fibers, since our experimental methods, while optimal for resolving charge movement kinetics, do not yield a precise measurement of the absolute ($\mu F/cm^2$) fiber capacitance (Beam and Donaldson, 1983).

Once the parameters that define the linear electrical properties of the fiber are chosen, the three kinetic parameters of charge redistribution, $\bar{\tau}$, $\bar{V}$, and k, remain to be fit. $\bar{V}$ and k (and also Q_{max}) were obtained by fitting the Boltzmann expression (Eq. 6*a*) to the steady state Q vs. V data of the individual fiber. The remaining parameter, $\bar{\tau}$, was varied until a visual best fit was obtained of the ON charge movement at 0 mV. With $\bar{\tau}$ chosen, the kinetics of the calculated ON and stepped OFF charge movements at all other potentials were completely constrained. The theoretical charge movements were calculated with a density of 30 nC/μF, which is typical of the density of mobile charge measured in our experiments. To critically compare their kinetics, we superimposed the calculated and measured charge movements. For this purpose, the theoretical charge movements were scaled in magnitude by Q_{max}/(30 nC/μF) ±5%, where 5% is comparable to the scatter of the actual Q vs. V data around the Boltzmann curve.

Convergence of the Model

The model employed in our calculations differs from that of Adrian and Peachey (1973) in that the annuli have equal areas, rather than being spaced at equal radial increments. We determined that convergence with the equal-area model required fewer than half as many annuli as the model with equal radial increments. Convergence is more rapid with the equal-area method, because both the linear capacitative load presented by an annulus and the nonlinear currents that it contributes are proportional to area. With equal radial increments, the inner annuli have small areas and thus contribute to the calculation time while having only a small effect on the time course of current flow from the surface into the first annulus.

One test of convergence was to compare the linear capacity transient predicted by the equal-area model, with the exact solution of the differential equation describing the propagation of potential within a fiber having a continuously distributed t-system:

$$K\frac{\partial^2 V}{\partial r^2} + \frac{K}{r}\frac{\partial V}{\partial r} = \frac{\partial V}{\partial t}, \tag{10}$$

where r is the radial distance from the center of the fiber, V is the voltage across the t-tubule membrane as a function of position and time, and K is a constant equal to $\bar{G}_l/\bar{C}_w$. For an exponentially rounded step in potential at the surface of the fiber, the solution to Eq. 10 is:

$$V(r, t) = 1 - \exp(-t/\tau_c) - 2\sum_1^\infty \frac{J_0(a_n r/a)[\exp(-a_n^2 Kt/a^2) - \exp(-t/\tau_c)]}{a_n J_1(a_n)(1 - Ka_n^2\tau_c/a^2)}, \tag{11}$$

where τ_c is the time constant of the command step on the surface of the fiber, J_0 and J_1 are Bessel functions of the first kind, and a_n are the zeroes of J_0 (see Appendix). With 12 annuli and an integration time increment of 0.5 μs, the potential as a function of time at four positions within the fiber, as predicted by the equal-area model, was in good agreement with the solution given by Eq. 11. (For this comparison, the access resistance was assumed to be zero.)

Another test of convergence was to compare the predictions of the equal-area model for differing time increments and numbers of annuli. Both the linear capacity transient and the charge movements calculated with 12 annuli were in good agreement with those calculated with 24 annuli. With 12 annuli, the time increment of 0.5 μs in Eq. 3 was shown to generate charge movements virtually identical to those generated with a time increment of 0.1 μs, and 0.5 μs was therefore used in all the calculations.

RESULTS

Fits of the Distributed Two-State Model to Measured Charge Movements

Figs. 1–3 compare charge movements predicted by the distributed two-state

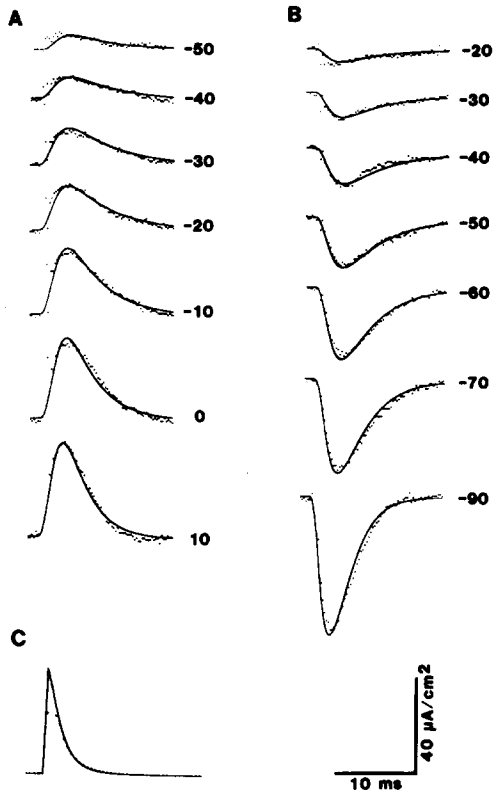

FIGURE 1. Comparison of charge movements predicted by the distributed two-state model, with charge movements measured in a fiber at 7°C. In this and the following two figures, theoretical curves are shown as solid lines. (*A*) Superposition of calculated and measured ON charge movements for depolarizations from −90 mV to the indicated test potentials. (*B*) Superposition of calculated and measured stepped OFF charge movements for repolarizations from 0 mV to the indicated test potentials. (*C*) Comparison of the calculated and measured linear capacity transient. The experimental linear capacity transient was measured as the current elicited by a depolarizing step from −135 to −90 mV. Theoretical charge movements were calculated according to Eqs. 1–9, with $\bar{V} = -30$ mV, $k = 10.5$ mV, $\bar{\tau} = 5.4$ ms, and $\bar{G}_1 = 13$ μS/cm. Details of the fitting procedure are given in the text. Experimental charge movements from muscle 99-2. Current and time calibrations apply to *A* and *B*; for *C*, the horizontal calibration = 5 ms, and the vertical calibration = 320 μA/cm².

model with charge movements measured experimentally at temperatures of 7 (Fig. 1), 15 (Fig. 2), and 25°C (Fig. 3, same fiber as in Fig. 1). As described in Methods, the first step in applying the model to a particular fiber was to adjust the parameters that define the passive properties of the t-system until a good fit

of the linear capacity transient was obtained. The fits of the model to experimental linear capacity transients are illustrated in Figs. 1*C*, 2*C*, and 3*B*. The parameters used to calculate these theoretical linear capacity transients are summarized in Tables I and II. The second step in applying the model was to obtain values for k and $\bar{V}$ by fitting the Boltzmann expression, Eq. 6*a*, to the steady state Q vs. V data of the fiber. The values of k and $\bar{V}$ constrain the voltage dependence of the rate constants for charge redistribution, but not their absolute

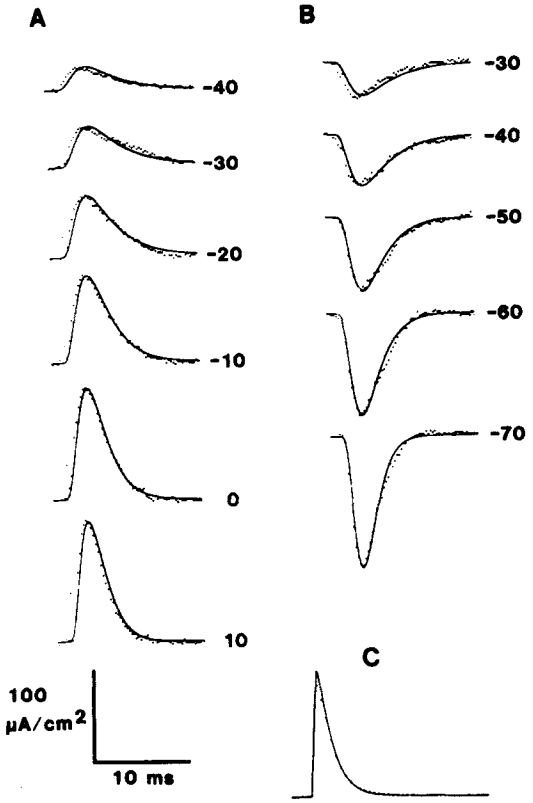

FIGURE 2. Fits of the distributed two-state model to charge movements measured at 15°C. (*A*) Predicted and measured ON charge movements. (*B*) Predicted and measured stepped OFF charge movements. (*C*) Predicted and experimental linear capacity transients. Muscle 99-1: $\bar{V} = -35$ mV; $k = 8.5$ mV; $\bar{\tau} = 3.2$ ms; $\bar{G}_1 = 10$ μS/cm. Current and time calibrations apply to *A* and *B*; for *C*, the horizontal calibration = 5 ms, and the vertical calibration = 400 μA/cm².

magnitude. This last free parameter was determined by adjusting $\bar{\tau}$ until the theory fit the experimental charge movement at a single test potential (0 mV). The charge movements at all other test potentials were then calculated with no additional adjustment of parameters. The values of k, $\bar{V}$, and $\bar{\tau}$ used to calculate the charge movements in Figs. 1–3 are summarized in Table II.

Fig. 1 illustrates that ability of the theory to fit ON and stepped OFF charge movements measured at 7°C. The theory gives a good account of both ON

charge movements (*A*), which were measured for depolarizing steps from −90 mV to test potentials ranging from −50 to +10 mV, and stepped OFF charge movements (*B*), which were measured for repolarizing steps from 0 mV to test potentials ranging from −20 to −90 mV. Fig. 2 demonstrates that the theory gives a similarly good account of ON (*A*) and stepped OFF (*B*) charge movements at 15°C, and Fig. 3 shows that the calculated curves agree well with ON charge

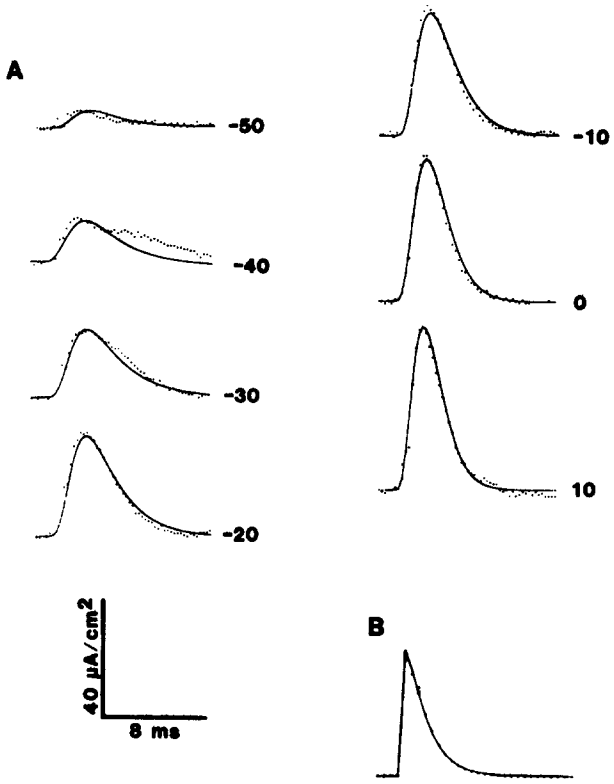

FIGURE 3. Fits of the distributed two-state model to ON charge movements at 25°C. Same muscle fiber as in Fig. 1. (*A*) Comparison of calculated and measured ON charge movements. The prominent bump on the falling phase of the charge movement at −40 mV may represent the Q_γ component of charge movement that has been described for frog muscle. (*B*) Calculated and measured linear capacity transients. Muscle 99-1: $\bar{V} = -30$ mV; $k = 8.5$ mV; $\bar{\tau} = 2.2$ ms; $\bar{G}_1 = 13$ μS/cm. Current and time calibrations apply to *A*; for *B*, the horizontal calibration = 4 ms, and the vertical calibration = 200 μA/cm².

movements measured at 25°C. No attempt was made to fit the stepped OFF charge movements at 25°C because they were contaminated by ionic currents. The fits of the model shown in Figs. 1–3 are typical of the fits obtained of ON and stepped OFF charge movements measured in other fibers at temperatures ranging from 3 to 25°C. Two consistent, small deviations between the theory and data should be noted. The first is that for small voltage steps, the experi-

TABLE I

Physical and Electrical Constants for Surface and Tubular Membranes

a, fiber radius	32 μm
C_w, capacitance per unit area of surface and t-tubule membrane	1 μF/cm²
G_l, conductivity of lumen	8.7 mS/cm*
ρ, fraction of fiber volume occupied by tubules	0.003
ζ, volume-to-surface ratio of tubules	10^{-6} cm
σ, network geometric factor	0.5
R_a, access resistance	60 Ω·cm²
Constants and parameters based on these units:	
$\bar{C}_w$, capacitance of t-system per unit volume = $C_w\rho/\zeta$	3,000 μF/cm³
$\bar{G}_l$, conductance of lumen of t-system per unit volume = $G_l\rho\sigma$	13 μS/cm*
C_t, capacitance of t-system per unit area of fiber surface = $a\bar{C}_w/2$	4.8 μF/cm²
Total capacitance per unit area of fiber surface	5.8 μF/cm²

* Typical values for fibers at 15°C.

mental charge movements rise slightly more rapidly than predicted by the theory. This mismatch of the rising phases is present both for ON charge movements (e.g., in Figs. 1*A*, 2*A*, and 3*A* at test potentials in the range −50 to −30 mV) and for stepped OFF charge movements (e.g., in Fig. 2*B* at −30 mV). Possible sources of this small mismatch of the rising phase are considered in the Discussion. The second discrepancy is that at test potentials near $\bar{V}$, the decay of ON charge movements frequently showed a "bump" of current not accounted for by the theory (e.g., Fig. 2*A* at −30 mV and Fig. 3*A* at −30 and −40 mV). The bump may represent the Q_γ component of charge movement (see Discussion in Simon and Beam, 1985). The bump at −40 mV in Fig. 3*A* is the largest observed in any of the fibers we have studied.

Despite the presence of these small discrepancies, it is clear that the theory gives a good description of both the rising and falling phase of charge movements. Thus, tubular delays, by altering the measured kinetics of a simple two-state reaction, can account for the experimentally observed rising phase and delay to peak, and a multiple-state reaction scheme for the mobile charge is not necessary.

Effect of Access Resistance on the Time Course of Charge Movement

In order to model action potentials in frog skeletal muscle fibers, Adrian and Peachey (1973) found it necessary to include an access resistance in their concentric annular representation of the t-system. The access resistance (R_a,

TABLE II

Constants Used for Calculating the Charge Movements Shown in Figs. 1–3

Muscle number	Temperature	$\bar{G}_l$	$\bar{V}$	k	$\bar{\tau}$
	°C	μS/cm	mV	mV	ms
99-2	7	10	−30	10.5	5.4
99-1	15	10	−35	8.5	3.2
99-2	25	13	−30	8.5	2.2

$\Omega \cdot cm^2$) separates the lumen of the t-system from the bulk fluid surrounding the fiber. The physical basis of R_a is uncertain. It has been suggested that R_a arises from a narrowing or tortuosity of the t-tubules near the surface of the fiber (Adrian and Peachey, 1973), and from the relatively small number of t-tubular openings onto the surface (Huxley and Taylor, 1958). However, Valdiosera et al. (1974) have argued that an appreciable access resistance is inconsistent with their impedance measurements on frog skeletal muscle fibers. Thus, we investigated the effect of varying R_a. For any given value of R_a between 0 and 150 $\Omega \cdot cm^2$, a corresponding value for $\bar{G}_1$ could be determined such that the model

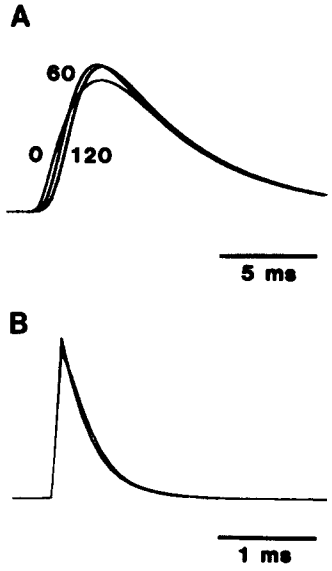

FIGURE 4. The effect of changing the access resistance (R_a) on the time course of calculated charge movements. (*A*) Charge movements calculated for a depolarization from −90 to −20 mV, $\bar{\tau} = 3$ ms, and access resistances of 0, 60, and 120 $\Omega \cdot cm^2$, as indicated. The curve for $R_a = 60\ \Omega \cdot cm^2$ is the same theoretical charge movement as illustrated at −20 mV in Fig. 2*A*. (*B*) Linear capacity transients corresponding to each of the charge movements in *A*. For the different values of R_a, it was possible to adjust $\bar{G}_1$ such that the time course of the linear capacity transient remained approximately the same. The resulting values of $\bar{G}_1$ were 7, 13, and 30 μS/cm, respectively, for $R_a = 0$, 60, and 120 $\Omega \cdot cm^2$.

provided an accurate fit to the experimental linear capacity transient. Although equally good fits of the linear capacity transient are possible for a range of values for R_a, this is not the case for charge movement. Too small an access resistance results in calculated charge movements that rise too quickly and are too broad at half-height, whereas too high an access resistance yields charge movements that rise too slowly and are too narrow at half-height. The optimal value of R_a was found to be ~60 $\Omega \cdot cm^2$.

The effects of varying R_a are illustrated in Fig. 4*A*, which compares charge movements calculated with access resistances of 0, 60, and 120 $\Omega \cdot cm^2$. (The

charge movement calculated for $R_a = 60\ \Omega \cdot cm^2$ is the same one illustrated in Fig. 2 at −20 mV.) For each of the three values of R_a, a value was determined for $\bar{G}_l$ such that the time course of the calculated linear capacity transient remained about the same. Fig. 4*B* demonstrates that for access resistances of 0, 60, and 120 $\Omega \cdot cm^2$, lumen conductances of 7, 13, and 30 μS/cm, respectively, yielded capacity transients that were nearly identical and which would each have provided a good fit to the experimental linear capacity transient shown in Fig. 2*C*. However, neither the charge movement calculated with $R_a = 0$ nor that calculated with $R_a = 120\ \Omega \cdot cm^2$ provides as good a fit of the experimental charge movement in Fig. 2*A* as does the charge movement calculated for $R_a = 60\ \Omega \cdot cm^2$. This value is considerably smaller than the 150 $\Omega \cdot cm^2$ found by Adrian and Peachey (1973) to best describe action potentials in frog muscle fibers, but it is similar to the 50 $\Omega \cdot cm^2$ found by Heiny et al. (1983), who used concentric annuli to model anomalous rectification in the t-system of frog muscle. The model of Heiny et al. was constrained by both the electrical measurement of current flowing into the fiber and the optical measurement of potential within the t-system. Using impedance analysis, Valdiosera et al. (1974) found values for R_a of ~20, 40, and 130 $\Omega \cdot cm^2$, respectively, for frog muscle fibers bathed in normal Ringer, Ringer 2× hypertonic with sucrose, and Ringer 2.5× hypertonic with sucrose.

With an access resistance of 60 $\Omega \cdot cm^2$, the linear capacity transient in the omohyoid was best modeled with a $\bar{G}_l$ of ~13 μS/cm (assumed fiber radius of 32 μm and temperature of 15°C). This $\bar{G}_l$ is in good agreement with the value of 15 μS/cm used by Adrian and Peachey (1973) and with the 13.5 μS/cm used by Heiny et al. (1983).

Effect of Tubular Delay on Charge Movement Decay

One would expect tubular propagation delays to affect not only the rising phase of charge movement, but also the decay phase. As a means of estimating the magnitude of this effect, τ_{decay} was obtained by fitting a single exponential to the decay phase of theoretical charge movements using the same fitting procedure that was described for experimental charge movements in the previous paper (Simon and Beam, 1985). Fig. 5 plots, as a function of potential, τ_{decay} for theoretical ON (open symbols) or stepped OFF (filled symbols) charge movements calculated with $\bar{\tau}$ equal to 6 (squares), 3.5 (circles), or 2 (diamonds) ms. These values of $\bar{\tau}$ were chosen to generate charge movements that approximate those that would be measured experimentally at 5, 15, and 25°C, respectively. In the absence of tubular propagation delays, the charge movements would have decayed exponentially with a time constant given by Eq. 9. This time constant, τ_Q, is plotted in Fig. 5 both for $\bar{\tau} = 6$ ms (upper dashed curve) and for $\bar{\tau} = 2$ ms (lower dashed curve). (A plot of τ_Q for $\bar{\tau} = 3.5$ ms was omitted from Fig. 5 to avoid crowding the figure.) τ_Q can be thought of as the time constant with which charge movements would decay for an instantaneous step in voltage. Tubular delays cause τ_{decay} to be slower than τ_Q, with the relative magnitude of the slowing depending on both temperature and potential. At a given temperature, the slowing of decay is least at −30 mV, which is the value of $\bar{V}$ used for these

calculations, and greatest at −90 mV, which is the potential farthest from $\bar{V}$ for which charge movements were calculated. The relative slowing is minimal for the slowest of the theoretical charge movements, those calculated for a temperature of 5°C. At 5°C, τ_{decay}/τ_Q varies from a minimum of 1.08 (at −30 mV) to a maximum of 1.22 (at −90 mV). For the calculated charge movements at 15°C, τ_{decay}/τ_Q varies from 1.19 at −30 mV to 1.48 at −90 mV. Thus, tubular

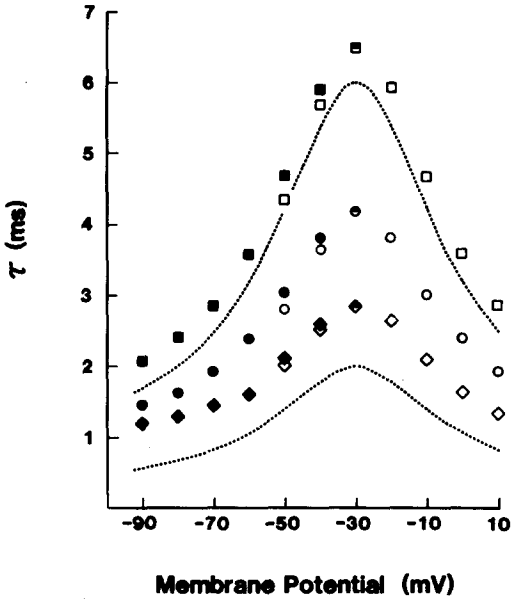

FIGURE 5. The voltage dependence of τ_{decay} at 5, 15, and 25°C. Values of τ_{decay} were determined by fitting exponentials with a least-squares procedure (Simon and Beam, 1985) to the falling phase of charge movements calculated with the distributed two-state model. Open symbols were obtained from ON charge movements and filled symbols from stepped OFF charge movements. The charge movements were calculated with $\bar{V} = -30$ mV, $k = 8.5$ mV, $\bar{G}_l = 13$ μS/cm (which yields a time constant of ~0.8 ms for the slow phase of the linear capacity transient), and $\bar{\tau} = 6$ (squares), 3.5 (circles), or 2 ms (diamonds). The values chosen for $\bar{\tau}$ correspond to a Q_{10} of ~1.75, and result in computed charge movements similar to those measured experimentally at 5, 15, and 25°C. The voltage dependence of τ_Q, the time constant of the underlying charge redistribution that is given by Eq. 9, is plotted for $\bar{\tau} = 6$ (upper broken curve) and 2 ms (lower broken curve). For a plot of τ_{decay} vs. potential for experimental charge movements at 7, 15, and 25°C, see Fig. 8 of Simon and Beam (1985).

propagation delays slow the decay of charge movement by ≤50% at 15°C and below. At 25°C, however, where τ_Q becomes comparable to τ_{lct} (the time constant of the linear capacity transient), the slowing of charge movement decay is already appreciable at −30 mV ($\tau_{decay}/\tau_Q = 1.44$) and is even greater at −90 mV ($\tau_{decay}/\tau_Q = 2.10$).

At both 5 and 15°C, τ_{decay} is slower than τ_Q, but the ratio τ_{decay}/τ_Q does not vary appreciably with voltage. Thus, for the charge movements calculated at

these temperatures, the constant field expression, Eq. 9, describes not only the potential dependence of τ_Q but also that of τ_{decay}. Since the kinetics of the calculated and experimental charge movements are in good agreement, it is also the case that the constant field expression gives a good description of τ_{decay} for experimental charge movements measured in the omohyoid muscle at temperatures of 15°C and below. At 25°C, however, τ_{decay}/τ_Q varies considerably with potential and, as a result, τ_{decay} shows less dependence on potential than predicted by the constant field expression.

One prediction of the distributed two-state model that mirrors the experimental data involves the behavior of τ_{decay} for ON and stepped OFF pulses to the same test potential. In Fig. 5, τ_{decay} was determined for both ON (τ_{ON}) and stepped OFF ($\tau_{stepped\ OFF}$) charge movements at −30, −40, and −50 mV. At all three potentials, τ_{ON} and $\tau_{stepped\ OFF}$ are similar, but at −50 and −40 mV, $\tau_{stepped\ OFF}$ is slightly larger than τ_{ON}. The explanation is that during the time when potential is changing during a step from −90 to either −50 or −40 mV, τ_Q is always faster than it will be at the final potential. Thus, the average τ_Q during the depolarizing step is smaller than τ_Q at the final potential. For a stepped OFF pulse to the same potential, however, voltage must pass through $\bar{V}$, where τ_Q is slower than at −40 or −50 mV. Thus, during the time when potential is changing, the average τ_Q is larger for the stepped OFF charge movement. The observation that at a given potential the calculated $\tau_{stepped\ OFF}$ is greater than τ_{ON} is in agreement with the experimental data in Fig. 8 of Simon and Beam (1985).

Voltage Dependence of the Rate Constants of Charge Redistribution

The theoretical charge movements illustrated in this paper were calculated with rate constants having a voltage dependence given by Eq. 8, the constant field expression, which can be derived from a model in which the redistribution of charge between two states is governed by diffusion and a constant intramembrane field that is proportional to the transmembrane potential (Chandler et al., 1976; Benz and Zimmerman, 1983). However, the applicability of such a continuum electrodiffusion description to the molecular rearrangements of the protein(s) that probably mediates E-C coupling is questionable. Thus, we also calculated charge movements with rate constants that have a voltage dependence derived from the Eyring rate theory description of a charge moving between two energy wells separated by a barrier (Adrian, 1978). In the case where the barrier is equidistant between the wells, the rate constants are given by:

$$\alpha = \bar{\alpha} \exp(\phi/2); \qquad \beta = \alpha \exp(-\phi), \tag{12}$$

and the time constant of decay by:

$$\tau = 1/(\alpha + \beta) = \bar{\tau}/\cosh(\phi/2). \tag{13}$$

Fig. 6 compares the predictions of Eyring rate theory, Eq. 13, and the constant field expression, Eq. 9, for the voltage dependence of τ. The τ predicted by Eyring rate theory (broken curve) shows a steeper voltage dependence than that predicted by the constant field expression (smooth curve). This steeper voltage dependence of the rate constants given by Eyring rate theory results in calculated

charge movements that decay too rapidly at potentials far from $\bar{V}$, when compared with experimental charge movements.

If the Eyring theory is modified to include nonlinear effects of the external field on the potential energy profile within the membrane (Stevens, 1978; Almers, 1978), it is then possible to obtain a voltage dependence for τ similar to that predicted by the constant field expression. In particular, if the height of the barrier depends on potential raised to both the first and the second powers (ϕ and ϕ^2), then the rate constants become:

$$\alpha = \bar{\alpha} \exp(\phi/2 - d\phi^2/4); \qquad \beta = \alpha \exp(-\phi), \tag{14}$$

and t is given by:

$$\tau = \bar{\tau} \exp(d\phi^2/4)/\cosh(\phi/2), \tag{15}$$

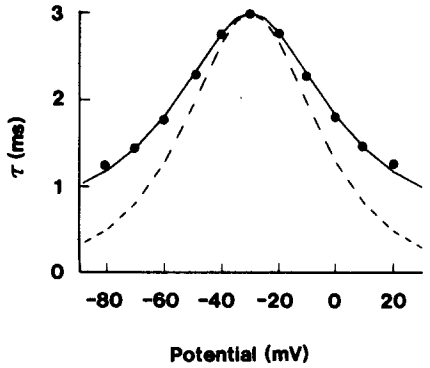

FIGURE 6. A comparison of the voltage dependence of $\tau(V)$ predicted by the constant field expression, "linear" Eyring rate theory, and "nonlinear" Eyring rate theory. The solid line is a plot of Eq. 9, which is derived from a constant field diffusional model, and the broken line is a plot of Eq. 13, which is derived from "linear" Eyring rate theory for the movement of charge between two potential wells separated by a single energy barrier with a height depending linearly on potential. The filled circles are derived from "nonlinear" Eyring rate theory, Eq. 15, in which the barrier height depends on both the first and second powers of potential. The illustrated points were obtained with $d = 0.15$ in Eq. 15, where d is the coefficient of the potential squared term. Over the potential range from −90 to +20 mV, the nonlinear Eyring rate theory is nearly indistinguishable from the constant field expression. For all three plots, $\bar{V} = -30$ mV, $k = 10$ mV, and $\bar{\tau} = 3$ ms.

where d is the coefficient of the ϕ^2 term. With a suitable choice for d, Eq. 15 can be made to approximate the constant field expression over the potential range where charge movements have been measured. This is illustrated in Fig. 6, where the filled circles are a plot of Eq. 15 for $d = 0.15$. Thus, either the constant field expression or Eyring rate theory with a barrier height that depends nonlinearly on potential yields rate constants with the appropriate voltage dependence to account for the experimentally measured charge movements.

The magnitude of the nonlinear potential term in Eq. 15 can be compared with the other terms as follows. The energy barrier required to give rate constants

of the order of 160/s, corresponding to the $\bar{\tau}$ of 3 ms that was used to generate the curves in Fig. 6, would be ~24 *RT* units high. For the linear Eyring rate theory with $\bar{V} = -30$ mV and $k = 10$ mV, the barrier height at +10 mV differs from that at $\bar{V}$ by 2 *RT*. The inclusion of the ϕ^2 dependence with $d = 0.15$ in Eq. 15 increases the barrier height at +10 mV by 0.6 *RT*.

Andersen and Fuchs (1975) have used a continuum electrodiffusion treatment to describe the kinetics of movement of the lipophilic anion tetraphenylborate absorbed into a lipid bilayer separating two aqueous solutions. They numerically integrated the Nernst-Planck diffusion equation assuming a particular nonlinear potential profile, which included a large central image-force barrier, and a deep, narrow minimum near each of the two interfaces between the bilayer and aqueous solution. The resulting expression is identical to Eq. 15, the nonlinear Eyring theory. In the treatment of Andersen and Fuchs, the coefficient of the potential

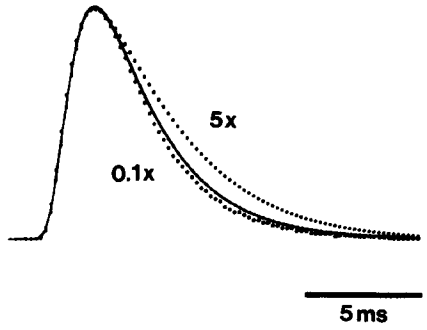

FIGURE 7. The effect of charge density on the kinetics of charge movement. Theoretical ON charge movements were calculated with identical parameters except for the charge density, which for the solid trace was 30 nC/μF, a typical physiological density, and for the dotted traces was 0.1× and 5× this density. To facilitate comparison of kinetics, the charge movements were scaled so that their peaks coincided. τ_{decay} was 3.1, 3.2, and 4.3, ms, respectively, for charge densities of 0.1×, 1×, and 5× physiological. Test pulse = 0 mV, $\bar{G}_1 = 13$ μS/cm, $\bar{V} = -30$ mV, $k = 10$ mV, $\bar{\tau} = 3$ ms.

squared term was found to be related to the shape of the central barrier and the width of the membrane.

Effect of Charge Density on Tubular Propagation Delays

The theoretical charge movements illustrated in Figs. 1–4 were calculated with the density of the mobile charge assumed to be 30 nC/μF, which is representative of the values measured experimentally in the omohyoid muscle (Simon and Beam, 1985). The presence of this quantity of mobile charge means that a step in potential from −90 to 0 mV requires not only 90 nC/μF to charge the linear capacitance of the fiber, but also 30 nC/μF to move the nonlinear charge. Thus, the question arises whether the presence of this quantity of charge slows the propagation of voltage within the t-system. As a means of addressing this issue, we calculated charge movements, varying the total density of the mobile charge. The assumption underlying this approach is that if the mobile charge were itself

slowing tubular propagation, then decreasing the charge density would speed propagation and hence speed the kinetics of the computed charge movement. Fig. 7 illustrates three charge movements calculated with charge densities of 0.1×, 1×, and 5× the standard density, but with otherwise identical parameters, for a step from −90 to 0 mV. To facilitate the comparison of kinetics, the records were scaled so that the peaks coincided. A comparison of the records with 1× (continuous curve) and 0.1× standard density shows that a 10-fold reduction in density only slightly speeds the decay of the calculated charge movement. Specifically, an exponential fitted to the decay phase of the records had a time constant of 3.2 ms for the 1× density and 3.1 ms for the 0.1× density. An additional 10-fold reduction, to 0.01×, had no further effect on the time constant. However, when the density was increased from 1× to 5×, the kinetics were significantly slowed and τ_{decay} increased to 4.3 ms.

The computations illustrated in Fig. 7 are based on parameters that describe the charge movements that would have been measured experimentally at ~15°C. A similar result was obtained for computed charge movements approximating those that one would expect to measure at temperatures ranging from 5 to 37°C: decreasing the charge density 10-fold from its physiological value had only a small effect on the propagation velocity, whereas increasing the density to 5× physiological slowed propagation.

This result is significant with regard to the experimental procedure used to measure charge movements. In order to measure charge movements, a control current, elicited by a step in voltage over a potential range where little nonlinear charge moves, is scaled and subtracted from the test current elicited by a step in voltage that does move charge. The validity of this procedure requires that the kinetics of the voltage change within the t-system be the same during the control and test steps. Our calculations with the distributed two-state model suggest that this condition is met and that charge movement at its physiological density in the omohyoid muscle has little effect on the passive propagation of voltage in the t-system.

DISCUSSION

This paper describes a simple physical model that can account for many of the properties of charge movement observed in mammalian skeletal muscle. In the model, a mobile charge obeying a two-state reaction scheme is located throughout an electrically distributed t-system. The model accurately fits the time course of ON, OFF, and stepped OFF charge movements at temperatures ranging from 3 to 25°C and test potentials that span the range from −90 to +10 mV. The model reproduces the experimental observation that the Q_{10} of charge movement decay depends on both temperature and test potential, and accounts in particular for the observation that at test potentials far from $\bar{V}$, raising the temperature from 15 to 25°C has only a small effect on the kinetics of charge movement. The ability of the model to fit not only the falling phase of charge movements but also the rising phase suggests that the rising phase is a consequence of the distributed nature of the t-system, which functions to slow the propagation of potential. Thus, a simple two-state model appears sufficient to describe the underlying charge redistribution process.

Na Gating Current on the Surface of the Fiber

In principle, one would expect Na channel gating current to be present as a component of the total asymmetry current measured in muscle, but the contribution of Na gating current to our records appears to be small. Measured in frog muscle with the rapid, vaseline-gap voltage-clamp technique, Na gating current is seen as a spike-like transient of current that precedes charge movement (Campbell, 1983). To investigate the effects of Na gating current on calculated charge movements, the distributed two-state model was modified to include Na gating current on the surface of the fiber. For this calculation, the potential on the surface of the fiber was assumed to change exponentially with a time constant of 350 μs, which corresponds to that observed experimentally (see Methods). Even with this relatively slow change in potential, the calculated Na gating current appeared as a distinct spike on the rising phase of the charge movement. No such spike-like component appears to be present in our records of charge movement in rat muscle (Simon and Beam, 1985). Furthermore, the rising phases of an ON charge movement at +10 mV and an OFF charge movement at −90 mV are nearly identical and can be well fitted by the model without Na gating current. In frog muscle, a 31-ms depolarizing step to +10 mV would immobilize more than two-thirds of the Na gating current (Campbell, 1983). Thus, one would expect the contribution of Na gating current to be nearly three times larger for the ON charge movement than for the OFF. The similarity of the rising phases of ON and OFF charge movements thus suggests that very little Na gating current is present in either.

The apparent absence of significant Na channel gating charge is consistent with estimates of the amount of charge expected. Pappone (1980) determined a peak Na conductance of 40–50 mS/cm^2 in rat fast-twitch muscle fibers at 12°C. After correction for contraction, the total linear capacitance of the fibers averaged 5.9 μF/cm^2 of surface membrane. Under the assumptions that about half the total Na channels are open at the peak of current (Sigworth, 1980), that the single Na channel conductance is 18 pS (Sigworth and Neher, 1980), and that the equivalent of six charges moving across the membrane is associated with the gating of each channel (Hodgkin and Huxley, 1952), then the Na gating charge would be ~1 nC/μF. In rabbit fast-twitch skeletal muscle, a direct measurement indicates that 1.7 nC/μF of Na channel gating charge is present (D. T. Campbell, personal communication). Thus, the estimated Na channel gating charge is no more than 6% of Q_{max}, which could easily have been missed in our measurements.

Passive Properties of the T-System

The solutions used for the measurement of charge movements reduce the conductance of the fiber membrane to a low level. Thus, for simplicity, we have assumed that the leak conductance across the t-tubular wall (G_{wall}) is zero. G_{wall} for omohyoid muscle fibers under our experimental conditions can be estimated from the measured space constant of ~2 mm, an assumed fiber radius of 32 μm, and an assumed internal resistivity of 220 Ω·cm (cf. Hodgkin and Nakajima, 1972), which yield R_m = 5,500 Ω·cm^2 (normalized per unit area of fiber surface). If we assume that the surface and tubular membranes have equal specific leak

conductance, this value of R_m is equivalent to a G_{wall} of 0.032 mS/cm^2 (normalized per unit area of membrane) for $\bar{G}_l$ = 13 μS/cm. We examined the effect of a nonzero G_{wall} and determined that the amplitude and time course of a charge movement calculated for a step from −90 to 0 mV were virtually identical for a G_{wall} of 0 and 0.032 mS/cm^2. A further 10-fold increase in G_{wall}, to 0.32 mS/cm^2, reduced the amplitude of the calculated charge movement by ~30% but had little effect on its time course. This latter value of G_{wall} yields an R_m of 600 $\Omega \cdot$ cm^2, nearly as low as the values reported for rat EDL (Camerino and Bryant, 1976) and diaphragm (Palade and Barchi, 1977) muscle fibers in physiological solutions at 37°C. Hence, it is clear that under the experimental conditions used to measure charge movements, G_{wall} is sufficiently small that it can be neglected.

In fitting the model, we used the same values for the geometric parameters of the t-system (Table I) used by Adrian and Peachey (1973) for frog muscle. We are unaware of morphometric measurements of the t-system in the rat omohyoid muscle, although such measurements do exist for other mammalian fast-twitch muscles. For the mouse EDL, Luff and Atwood (1971) reported that ρ = 0.4%, and that the surface area of the t-system, relative to the area of the fiber surface, is 3.1 cm^2/cm^2 for a 30-μm-diam fiber; from these, one calculates that $\zeta = 0.97 \times 10^{-6}$. Other values reported in the literature include ρ = 0.27% and $\zeta = 1.9 \times 10^{-6}$ for the vastus muscle of the guinea pig (Eisenberg and Kuda, 1975), ρ = 0.28% and $\zeta = 1.6 \times 10^{-6}$ for fast-twitch fibers of the human quadriceps (Eisenberg, 1983), and ρ = 0.42% and $\zeta = 1.3 \times 10^{-6}$ for the rat EDL (Cullen et al., 1984). All of these are in reasonable agreement with the values of ρ = 0.3% and $\zeta = 10^{-6}$ that we have used. These latter values were chosen not only because they result in a good description of the time course of passive charging of the t-system (Figs. 1*C*, 2*C*, and 3*B*), but also because they yield a total fiber capacitance in good agreement with measured values. Specifically, they yield a total membrane capacitance of 5.8 μF/cm^2 (calculated for a 32-μm-radius fiber with a specific membrane capacitance of 1 μF/cm^2 of tubular or surface membrane). For comparison, the electrically measured values for rat fast-twitch muscles (EDL, sternomastoid) include 6.6 (Adrian and Marshall, 1977), 5.9 (Pappone, 1980), 5.1 (Hollingworth and Marshall, 1981), and 6.2 μF/cm^2 (Dulhunty and Gage, 1983).

The value of G_l in Table I is calculated from the fitted value of $\bar{G}_l$ assuming a network geometric factor of 0.5. Such a network geometric factor has the disadvantage that it can be evaluated only for specific geometric arrays, which cannot in general describe the t-system. Mathias et al. (1977) have shown that the network geometric factor can be replaced by τ, a tortuosity factor, which can be derived from morphometric measurements of the t-system. For frog twitch fibers, Mathias et al. give a value of 0.32 for τ. If one assumes that τ = 0.32 for the rat omohyoid muscle (we are unaware of the existence in the literature from mammalian fibers of the morphometric parameters necessary for the calculation of τ), then our estimate of G_l at 15°C changes from 8.7 to 13.6 mS/cm. This is the only effect of choosing a specific value for σ or τ since $\bar{G}_l$ is the parameter describing the luminal conductance that we vary to fit the measured capacity transients.

Charge Movement on the Surface of the Fiber

In the model presented here, charge movement was assumed to reside only in the t-system. A variation of the model, which included charge on the surface, was also investigated. This inclusion introduces an additional free parameter, the relative density of charge on the surface compared with that in the t-system. If for simplicity it is assumed that the surface and tubular densities are the same, it is then necessary to use a larger value for the access resistance, 100 $\Omega \cdot cm^2$, to obtain a good fit of the measured charge movements. Generally, the inclusion of charge on the surface was found to improve the fit of the rising phase for small depolarizations without substantially changing the fits for larger depolarizations. However, other models might also improve the fit. For example, the charge might be present only in the t-system but present at higher densities nearer the surface of the fiber. Our data do not allow us to choose between these possibilities. Nonetheless, it is clear that the fits are already excellent with the simple distributed two-state model.

APPENDIX

Radial Propagation of Voltage for a Rounded Step at the Surface

The solution to the radial cable equation (Eq. 10) for a unit step in potential on the surface of the fiber is given by (Adrian et al., 1969):

$$A(r, t) = 1 - 2 \sum_{1}^{\infty} \frac{\exp(-a_n^2 Kt/a^2) J_0(a_n r/a)}{a_n J_1(a_n)}, \tag{A1}$$

where J_0 and J_1 are Bessel functions of the first kind, a_n are the roots of $J_0(x) = 0$, a is the radius of the fiber, and $K = \bar{G}_1/\bar{C}_w$. The solution to Eq. 10 for an arbitrary potential change on the surface, $V(a, t)$, is:

$$V(r, t) = V(a, 0)A(r, t) + \int_0^t A(r, t - T)[dV(a, T)/dT]dT, \tag{A2}$$

where $A(r, t)$ is given by Eq. A1. Eq. A2 can be shown to satisfy Eq. 10 by simple substitution. If the voltage on the surface is rounded with a time constant τ_c:

$$V(a, t) = 1 - \exp(-t/\tau_c), \tag{A3}$$

then substitution of Eqs. A1 and A3 into Eq. A2 gives potential as a function of time and position for a rounded voltage step:

$$V(r, t) = 1 - \exp(-t/\tau_c) - 2 \sum_{1}^{\infty} \frac{J_0(a_n r/a)[\exp(-a_n^2 Kt/a^2) - \exp(-t/\tau_c)]}{a_n J_1(a_n)(1 - Ka_n^2 \tau_c/a^2)}.$$

We thank Dr. D. Campbell for suggestions on the work and for reading the manuscript.
This work was supported by the Muscular Dystrophy Association and NS-14901 from the National Institutes of Health. K.G.B. is the recipient of Research Career Development Award NS-00840.

Original version received 1 May 1984 and accepted version received 7 August 1984.

REFERENCES

Adrian, R. H. 1978. Charge movement in the membrane of striated muscle. *Annu. Rev. Biophys. Bioeng.* 7:85–112.

Adrian, R. H., and W. Almers. 1976. Charge movement in the membrane of striated muscle. *J. Physiol. (Lond.).* 254:339–360.

Adrian, R. H., W. K. Chandler, and A. L. Hodgkin. 1969. The kinetics of mechanical activation in frog muscle. *J. Physiol. (Lond.).* 204:207–230.

Adrian, R. H., and M. W. Marshall. 1977. Sodium currents in mammalian muscle. *J. Physiol. (Lond.).* 268:223–250.

Adrian, R. H., and L. D. Peachey. 1973. Reconstruction of the action potential of frog sartorius muscle. *J. Physiol. (Lond.).* 235:103–131.

Almers, W. 1978. Gating currents and charge movements in excitable membranes. *Rev. Physiol. Biochem. Pharmacol.* 82:96–190.

Andersen, O. S., and M. Fuchs. 1975. Potential energy barriers to ion transport within lipid bilayers. Studies with tetraphenylborate. *Biophys. J.* 15:795–830.

Beam, K. G., and P. L. Donaldson. 1983. A quantitative study of potassium channel kinetics from 1 to 37°C. *J. Gen. Physiol.* 81:485–512.

Benz, R., and U. Zimmerman. 1983. Evidence for the presence of mobile charges in the cell membrane of *Valonia utricularis. Biophys. J.* 43:13–26.

Camerino, D., and S. H. Bryant. 1976. Effects of denervation and colchicine treatment on the chloride conductance of rat skeletal muscle fibers. *J. Neurobiol.* 7:221–228.

Campbell, D. T. 1983. Sodium channel gating currents in frog skeletal muscle. *J. Gen. Physiol.* 82:679–701.

Chandler, W. K., R. F. Rakowski, and M. F. Schneider. 1976. A non-linear voltage dependent charge movement in frog skeletal muscle. *J. Physiol. (Lond.).* 254:245–283.

Cullen, M. J., S. Hollingworth, and M. W. Marshall. 1984. A comparative study of the transverse tubular system of the rat extensor digitorum longus and soleus muscles. *J. Anat.* 138:297–308.

Dulhunty, A. F., and P. W. Gage. 1983. Asymmetrical charge movement in slow- and fast-twitch mammalian muscle fibers in normal and paraplegic rats. *J. Physiol. (Lond.).* 341:213–231.

Eisenberg, B. R. 1983. Quantitative ultrastructure of mammalian skeletal muscle. *In* The Handbook of Physiology: Skeletal Muscle. L. D. Peachey and R. H. Adrian, editors. American Physiological Society, Bethesda, MD. 73–112.

Eisenberg, B. R., and A. M. Kuda. 1975. Stereological analysis of mammalian skeletal muscle. II. White vastus muscle of the adult guinea pig. *J. Ultrastruct. Res.* 51:176–187.

Heiny, J. A., F. M. Ashcroft, and J. Vergara. 1983. T-system optical signals associated with inward rectification in skeletal muscle. *Nature (Lond.).* 301:164–166.

Hodgkin, A. L., and A. F. Huxley. 1952. A quantitative description of membrane current and its application to conduction and excitation in nerve. *J. Physiol. (Lond.).* 117:500–544.

Hodgkin, A. L., and S. Nakajima. 1972. The effect of diameter on the electrical constants of frog skeletal muscle fibers. *J. Physiol. (Lond.).* 221:105–120.

Hollingworth, S., and M. W. Marshall. 1981. A comparative study of charge movement in rat and frog skeletal muscle fibers. *J. Physiol. (Lond.).* 321:583–602.

Horowicz, P., and M. F. Schneider. 1981. Membrane charge moved at contraction thresholds in skeletal muscle fibers. *J. Physiol. (Lond.).* 314:595–633.

Huxley, A. F., and R. E. Taylor. 1958. Local activation of striated muscle fibers. *J. Physiol. (Lond.).* 144:426–441.

Luff, A. R., and H. L. Atwood. 1971. Changes in the sarcoplasmic reticulum and transverse tubular system of fast and slow skeletal muscles of the mouse during postnatal development. *J. Cell Biol.* 51:369–383.

Mathias, R. T., R. S. Eisenberg, and R. Valdiosera. 1977. Electr properties of frog skeletal muscle fibers interpreted with a mesh model of the tubular sys.. .n. *Biophys. J.* 17:57–93.

Müntener, M., J. Gottschall, W. Neuhuber, A. Mysicka, and W. Zenker. 1980. The ansa cervicalis and the infrahyoid muscles of the rat. *Anat. Embryol.* 159:49–57.

Palade, P. T., and R. L. Barchi. 1977. Characteristics of the chloride conductance in muscle fibers of the rat diaphragm. *J. Gen. Physiol.* 69:325–342.

Pappone, P. A. 1980. Voltage-clamp experiments in normal and denervated mammalian skeletal muscle fibers. *J. Physiol. (Lond.).* 306:377–410.

Schneider, M. F., and W. K. Chandler. 1973. Voltage dependent charge movement in skeletal muscle: a possible step in excitation-contraction coupling. *Nature (Lond.).* 242:244–246.

Sigworth, F. J. 1980. The variance of sodium current fluctuations at the node of Ranvier. *J. Physiol. (Lond.).* 307:97–129.

Sigworth, F. J., and E. Neher. 1980. Single Na^+ channel currents observed in cultured rat muscle cells. *Nature (Lond.).* 287:447–449.

Simon, B. J., and K. G. Beam. 1983*a*. Charge movement in a fast-twitch skeletal muscle from rat. *Biophys. J.* 41:223–226.

Simon, B. J., and K. G. Beam. 1983*b*. Kinetics of charge movement in rat muscle are well-described by a first order reaction in a distributed t-system. *Biophys. J.* 41:395*a*. (Abstr.)

Simon, B. J., and K. G. Beam. 1985. Slow charge movement in mammalian skeletal muscle. *J. Gen. Physiol.* 85:1–19.

Stevens, C. F. 1978. Interactions between intrinsic membrane protein and electric field. An approach to studying nerve excitability. *Biophys. J.* 22:295–306.

Valdiosera, R., C. Clausen, and R. S. Eisenberg. 1974. Impedance of frog skeletal muscle fibers in various solutions. *J. Gen. Physiol.* 63:460–491.